Biomaterials Science

PAPER

View Article Online
View Journal | View Issue

Cite this: *Biomater. Sci.*, 2020, **8**, 673

A novel cell membrane-cloaked magnetic nanogripper with enhanced stability for drug discovery†

Yusi Bu,[a,b] Qi Hu,[a,b] Xiaolin Zhang,[a,b] Ting Li,[a,b] Xiaoyu Xie *[a,b] and Sicen Wang*[a,b]

Cell membrane-cloaked nanotechnology has attracted increasing attention owing to its unique bionic properties, such as specific recognition and biocompatibility conferred by the integrated membrane structure and receptors. However, this technology is limited by the dissociation of the cell membrane from its carrier. Here, we report a novel type of cell membrane-cloaked modified magnetic nanoparticle with good stability in drug discovery. High α_{1A}-adrenergic receptor (α_{1A}-AR) expressing HEK293 cell membrane-cloaked magnetic nanogrippers (α_{1A}/MNGs) were used as a platform for the specific targeting and binding of α_{1A}-AR antagonists as candidate bioactive compounds from traditional Chinese medicine (TCM). Furthermore, using a dynamic covalent bonding approach, α_{1A}/MNGs showed great stability with positive control drug recoveries of α_{1A}/MNGs showing almost no decline after use in five adsorption–desorption cycles. Moreover, the α_{1A}/MNGs possessed a unilamellar membrane with magnetic features and exhibited good binding capacity and selectivity. Ultimately, TCM and pharmacological studies of the bioactivity of the screened compounds confirmed the considerable targeting and binding capability of α_{1A}/MNGs. Application of aldehyde group modification in this drug-targeting concept further improved biomaterial stability and paves the way for the development of new drug discovery strategies. More importantly, the successful application of α_{1A}/MNGs provides new insights into methodologies to improve the integration of cell membranes with the nanoparticle platform.

Received 3rd September 2019,
Accepted 6th November 2019

DOI: 10.1039/c9bm01411j

rsc.li/biomaterials-science

Introduction

Magnetic nanoparticles (MNPs) have unique physicochemical characteristics and are increasingly being applied to various areas such as magnetic resonance imaging,[1,2] drug delivery,[3] cell tracking[4,5] and drug discovery.[6] In particular, their efficient magnetic capacity and large surface area have been utilized for drug discovery through rapid targeting and gripping of bioactive compounds from complex matrix materials such as traditional Chinese medicines.[7,8] Therefore, over the last decade, important progress in magnetic nanotechnology has led to significant advances in the discovery of important natural products.[6,9] It is worth mentioning that the coating of MNPs is the most important part of the design in the whole natural product discovery procedure. A suitable coating is a prerequisite that enables MNPs to effectively bind their targets by increasing specific targeting while decreasing binding with non-specific compounds in complex samples. Hence, an efficient and target-selective coating technology is urgently required. To this end, biomimetic design based on the functionalization of naturally occurring materials has aroused great interest. This approach provides nanoparticles with incredible specificity. Many types of molecules such as enzymes,[10] peptides,[11] proteins[12] and other micromolecules[13] have been investigated for the functionalization of the surface of MNPs to equip them with distinct selective properties. These bioinspired approaches, which are unique and robust means to potentially impart natural characteristic on synthetic systems, have yielded promising results. However, simple molecule functionalization approaches are not sufficient to simulate the extremely complex interfaces that occur *in vivo*. Additionally, the structure of these molecules may be altered compared to that of their native counterparts during the synthesis process *in vivo*. These changes may result in false positive or false negative results. Hence, new approaches that involve the functionalization of MNPs with effective surfaces in the biological environment are required to accomplish comprehensive biological tasks *in vivo*.

A biomimetic design strategy using cell membrane-derived vesicles as a functional coating has attracted increasing attention to address the aforementioned limitations of integrating

[a]*School of Pharmacy, Health Science Center, Xi'an Jiaotong University, Xi'an 710061, China. E-mail: xiexiaoyu@xjtu.edu.cn, wangsc@mail.xjtu.edu.cn*
[b]*Shaanxi Engineering Research Center of Cardiovascular Drugs Screening & Analysis, Xi'an, 710061, China*

†Electronic supplementary information (ESI) available. See DOI: 10.1039/c9bm01411j

one single type of biomolecule onto synthetic nanoparticles.[14–19] In this approach, design cues from nature are utilized to mimic essential forms of cell membranes, such as shape and flexibility in synthetic nanosystems. Thus, the integral surface structures of the source cells can be used to equip nanoparticles with the inherent properties of the molecules on those cell membranes. To date, the cell membrane-cloaked nanoparticle approach has provided a novel strategy for engineering nanoparticles with a functional biointerface and has been used for drug delivery,[20,21] imaging and photoactivatable therapy,[22,23] detoxification[24,25] and immune modulation.[24,26,27] Moreover, biomimetic nanoparticles have been exploited to screen and extract bioactive compounds for drug discovery, which has greatly improved the discovery efficiency of lead compounds from natural products compared to the results yielded using more traditional methods.[28–30] It has been demonstrated that membrane receptors, which are the main targets for drug-binding, play an important role in cell biointerfacing. Moreover, the effectiveness of at least 50% to 60% of pharmaceuticals is known to be critically dependent on the interaction with their specific cell membrane receptors.[31–33] Employed in this way, cell membrane-cloaked nanoparticle technology has shown great potential as a selective screening tool for drug discovery. However, the cell membrane-cloaked approach is limited by low extraction stability due to the dissociation of the cell membrane falling from the nanoparticle materials during use.[28,34] Hence, more stable and effective cell membrane-cloaked materials are urgently required to overcome these limitations.

In general, particles and cell membranes are bound by hydrophobic interactions,[35] which are too weak to withstand use in real applications, leading to dissociation of the cell membrane from the surface of materials. Recently, covalent bonding has emerged as an effective paradigm to ameliorate the poor stability of biomaterials.[36,37] It has been reported that aldehyde groups can react with amine groups of the surface of cells[36] to form a stable imine linkage without disruption under physiological conditions.[38] On the other hand, cell membranes are rich in phospholipids, some of which like phosphatidyl-serine and phosphatidyl-ethanolamine possess free amino groups that can form imine linkages. Inspired by this, nanoparticles have been covalently coupled to cell membranes by reaction between abundant surface aldehyde groups of nanoparticles and exposed amino groups on the surface of cell membrane phospholipids without disruption. This strategy is effective for the improvement of the stability of cell membrane-cloaked nanotechnology by incorporating the advantages of dynamic covalent bonding.

Here, we report a novel biomimetic cell membrane-cloaked magnetic nanogripper with enhanced stability achieved by means of covalent bonding for screening bioactive compounds from the traditional Chinese medicine (TCM), *Radix aconiti agrestis* (RAA). TCMs have attracted great attention due to their successful clinical applications and reliable therapeutic effects. As a rich source for discovering new drugs, TCMs and natural products have made a significant contribution to the treatment of many diseases.[39–41] Many biologically active compounds screened from TCMs including as taxol[42,43] and camptothecin[44,45] have effective therapeutic effects for many diseases. Thus, the screening and identification of active compounds from TCMs is a very important aspect of the development of treatments for a variety of diseases.

The α_{1A}-adrenergic receptor (α_{1A}-AR), which belongs to the G protein-coupled receptor superfamily, has a close relationship with benign prostatic hyperplasia, a common disease mainly affecting elderly men.[46] Therefore, cell membranes expressing high levels of α_{1A}-AR are implicated for the effective screening of α_{1A}-AR antagonists. In this study, HEK293 cells expressing high levels of α_{1A}-AR were used to provide a cell membrane substrate that specifically binds bioactive compounds, regardless of differences in chemical structures. In addition, we used an inner magnetic core to stabilize the cell membrane shell and enable rapid and targeted binding of compounds *via* magnetic extraction. We characterized the morphology, magnetic properties, adsorption capacity and selectivity of high α_{1A}-AR expressing HEK293 cell membrane-cloaked magnetic nanogrippers (α_{1A}/MNGs). Moreover, by means of dynamic covalent bonding, we improved the adsorption capacity and stability of α_{1A}/MNGs, with only a 3.4% decline in recovery after five adsorption–desorption cycles. These advanced-stability and targeting capabilities hold considerable promise for diverse biomedical applications. The functional modification technique of nanoparticles highlights an efficient approach toward the integration of biomaterials with nanoparticle platforms.

Experimental

Materials and reagents

Silica gel (ZEX-II, 5 μm, 200 Å) was purchased from Qingdao Meigao Chemical Co., Ltd (Qingdao, China). Calycosin, ononin and quercetin were purchased from Preferred Biological Technology (Chengdu, China). Nifedipine, valsartan, captopril and methoxamine were obtained from Nanjing Ange Pharmaceutical Co., Ltd (Jiangsu, China). Acetonitrile and methanol (HPLC-grade) were from Thermo Fisher Scientific (Pittsburgh, PA, USA). HQ injection (lot#: 1412223) was provided by Zhengda Co., Ltd (Zhejiang, China). Paraformaldehyde (PFA) was purchased from Tokyo Chemical Industry (Tokyo, Japan). Dulbecco's modified Eagle's medium (DMEM) and trypsin were obtained from Sigma (Saint Louis, MO, USA). Fluorescein isothiocyanate isomer (FITC) was purchased from Yi Sheng Bio. Tech. Co. (Shanghai, China). 1,1′-Dioctadecyl-3,3,3′,3′-tetramethylindocarbocyanine perchlorate (DiI) was purchased from Beyotime Bio. Tech. Co. (Shanghai, China). HEK293, a human embryonic kidney cell line, was purchased from the National Infrastructure of Cell Line Resource (Beijing, China).

Instrumentation

α_{1A}/MNGs and non-cell membrane-cloaked magnetic nanogrippers (MNGs) were fully characterized by transmission elec-

tron microscopy (TEM), dynamic light scattering (DLS), X-ray diffraction (XRD), Fourier transform infrared spectroscopy (FT-IR), vibrating sample magnetometry (VSM) and X-ray photoelectron spectroscopy (XPS). TEM characterization was performed with a JEOL JEM-2100HR transmission electron microscope (Tokyo, Japan). XRD patterns were investigated in the range of 2θ = 20–80° with an X-Ray diffractometer using Cu Kα1 radiation (PANalytical X'Pert, Netherlands). FT-IR results were obtained by using a Nicolet Nexus-670 FT-IR spectrometer. Magnetic properties were investigated by using a Lake Shore 7410 vibrating sample magnetometer (Westerville, OH, USA). XPS analysis was conducted using Thermo Fisher Scientific. DLS investigation was characterized using a Zetasizer Nano ZSE (Malvern, UK).

Preparation and characterization of α_{1A}/MNGs

Fe_3O_4 MNPs were synthesized using a previously described solvothermal method.[47] Briefly, $FeCl_3{\cdot}H_2O$ (3.60 g) and trisodium citrate (0.72 g) were dissolved in ethylene glycol (100 mL) and ultrasonicated. NaAc (4.80 g) was then added and the solution was stirred vigorously at 50 °C for 30 min. The hybrid was then sealed in a 100 mL capacity Teflon-lined stainless-steel autoclave and heated to 200 °C for 10 h. The final product was washed six times with methanol and water.

The Fe_3O_4@SiO_2 nanoparticles were synthesized according to a previously reported method[48] with a minor modification. In brief, 0.1 g of dispersed Fe_3O_4 MNPs were added to a mixture of ethanol (80 mL) and ultrapure water (12 mL), followed by the addition of ammonia aqueous solution (4 mL, 25%) and the mixture was stirred at 40 °C. TEOS (tetraethyl orthosilicate, 0.8 mL) was then added to the mixture. After stirring for 8 h, Fe_3O_4@SiO_2 nanoparticles were separated using an external magnetic field and washed six times with methanol and ultrapure water.

The Fe_3O_4@SiO_2@NH_2 nanoparticles were prepared by reacting with APTES (3-aminopropyl triethoxysilane). First, 0.4 g of Fe_3O_4@SiO_2 nanoparticles were dispersed in 50 mL of anhydrous toluene. After sonication for 30 min and the addition of 4 mL of APTES, the reaction was stirred for 24 h under N_2 protection at 120 °C. The resultant nanoparticles were then washed sequentially with anhydrous toluene, methanol and water. Then, 100 mg of Fe_3O_4@SiO_2@NH_2 nanoparticles were immersed in 100 mL of (2% v/v) glutaraldehyde solution (pH 11) and stirred for 1 h at room temperature. After washing with water to neutral pH and drying under vacuum, Fe_3O_4–CHO nanoparticles were synthesized.

The HEK293 cell line, which expresses high levels of α_{1A}-AR, was used in this study to minimize adsorption of non-specific compound binding to the cell membrane. Cells were cultured in DMEM containing 100 U mL^{-1} streptomycin, 10% fetal bovine serum, 300 mg L^{-1} geneticin and 100 U mL^{-1} penicillin. Cells were cultured at 37 °C in a humidified atmosphere under 5% CO_2. In the exponential growth phase, cells were collected and washed three times with phosphate buffered saline (PBS, pH 7.4) for the preparation of α_{1A}/MNGs.

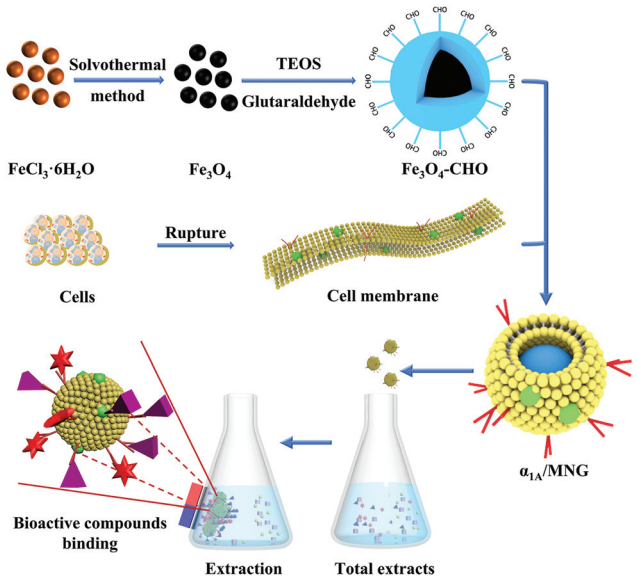

Fig. 1 Schematic illustration of the high α_{1A}-adrenergic receptor (α_{1A}-AR) expressing HEK293 cell membrane cloaked Fe_3O_4–CHO nanoparticles as nanogrippers for bioactive compound extraction.

The α_{1A}/MNG preparation process is illustrated in Fig. 1. Cell membranes were isolated according to previously reported methods.[28,49] After three repeated washes with PBS, the harvested cells were resuspended in 50 mmol L^{-1} Tris-HCl (pH 7.4) and ruptured by three cycles of ultrasonication (42 kHz, 100 W) for 30 min. The crude membrane precipitate was then washed three times with 10 mL of PBS by centrifugation at 12 000*g*, 4 °C for 20 min and finally suspended in PBS. The α_{1A}/MNGs were finally prepared by mixing sufficiently dispersed Fe_3O_4–CHO nanoparticles with the cell membrane suspension at 4 °C under vacuum and with ultrasonication. The MNGs were prepared under the same conditions with the replacement of cell membrane solution with PBS (pH 7.4).

The α_{1A}/MNGs were then subjected to confocal microscopy (Leica TCS SP5, Wetzlar, Germany) of fluorescently labeled components. Before coating, the lipid bilayer of the cell membrane suspension was labeled with DiI (red) by mixing at 4 °C for 40 min. FITC solution was added to the Fe_3O_4@SiO_2 reaction system to prepare Fe_3O_4–CHO/FITC (green) nanoparticles. Subsequently, α_{1A}/MNGs and MNGs were prepared as described previously. For FITC and DiI imaging, we used excitation wavelengths of 488 and 549 nm, respectively, and emission filters at 525 nm and 565 nm for FITC and DiI, respectively.

Stability test of α_{1A}/MNGs

A total of 50 mg of α_{1A}/MNGs or high α_{1A}-AR expressing HEK293 cell membrane-cloaked Fe_3O_4–OH nanoparticles (α_{1A}/Fe_3O_4–OHs) was added to tamsulosin solution. The mixture was then sonicated and shaken for 20 min at 37 °C. The α_{1A}/MNGs were separated using a magnet and washed with 5 mL of 0.1% acetic acid solution with sonication for 20 min to

decrease non-specific interactions. After collecting the washing solvent, 5 mL of 1% acetic acid solution was added to α_{1A}/MNGs with sonication for 20 min to completely remove the captured compounds. The washing solvent and eluent were then lyophilized to dryness and the residues were redissolved in 0.5 mL of methanol for further HPLC analysis.

Binding experiments

The isothermal adsorption properties of α_{1A}/MNGs were assessed by adding 5.0 mg of α_{1A}/MNGs or MNGs into a series of concentrations of tamsulosin from 60 to 3500 mg L^{-1} (1 mL) using 2 mL centrifuge tubes. All mixtures were sealed and shaken at 37 °C for 2 h. After separation using a magnetic field, supernatant solutions were analyzed by HPLC to determine tamsulosin concentrations.

The adsorption capacity (Q) was calculated according to eqn (1):

$$Q = \frac{(C_0 - C_e) \times V}{m} \quad (1)$$

where Q (mg g^{-1}) is the adsorption quantity of tamsulosin to α_{1A}/MNGs or MNGs, C_0 (mol L^{-1}) is the original concentration of tamsulosin before adsorption, C_e is the tamsulosin concentration of the supernatant after adsorption, V (mL) is the volume of the initial tamsulosin solution and m (g) is the mass of α_{1A}/MNGs or MNGs. All experiments were conducted in triplicate.

Real application

RAA was purchased from the Xi'an medicine market (Xi'an, China). In order to obtain more constituents, 10 g of RAA was ground into a powder and refluxed in 100 mL of ethanol (60%, v/v) for 2 h. The total extract was filtered using a Büchner funnel and concentrated to a dark brown mass, which was redissolved in the sample solution for use in all extraction procedures. Similarly, 50 mg of α_{1A}/MNGs was added to RAA solution. The mixture was sonicated and shaken for 20 min at 37 °C. The α_{1A}/MNGs were separated using a magnet and washed with 5 mL of 0.1% acetic acid solution with sonication for 20 min to decrease non-specific interactions. After collecting the wash solvent, 5 mL of 1% acetic acid solution was added to α_{1A}/MNGs with sonication for 20 min to completely remove the captured compounds. The wash solvent and eluent were lyophilized to dryness and the residues were redissolved in 0.5 mL of methanol for further HPLC analysis.

Animals

Sprague Dawley rats and healthy male New Zealand white rabbits were obtained from the Animal Center of Xi'an Jiaotong University (Xi'an, China, Production Certificate No. SYSK [Shan] 2007-003). All animal procedures were performed in accordance with the Guidelines for Care and Use of Laboratory Animals of Xi'an Jiaotong University and approved by the Animal Ethics Committee of Xi'an Jiaotong University.

In vitro vascular ring tension study

To investigate the pharmacological effects of bulleyaconitine A and benzoylhypacoitine, Sprague Dawley rat antral circular smooth muscle strips were isolated and mounted in Multi Myograph System-610M (Danish Myo Technology A/S, Aarhus, Denmark) organ chambers individually filled with Krebs buffer (pH 7.4). Tissues were maintained at 37 °C and aerated with continuous 95% O_2 and 5% CO_2. Each muscle strip was exposed to 4 nmol L^{-1} for 60 min to allow equilibration. Krebs solution was renewed every 20 min throughout the experiment. Subsequently, tissues were pre-contracted by the addition of 60 mmol L^{-1} K^+-rich Krebs solution and washed with Krebs solution three times to investigate the *in vitro* bioactivity of strips. After full stimulation with phenylephrine, each strip was treated with different concentrations of bulleyaconitine A, benzoylhypacoitine and tamsulosin from 1×10^{-8} to 1×10^{-4} mol L^{-1}. The concentration–response curves were then generated.

In vitro prostatic smooth muscle strip tension test

The pharmacological effects of bulleyaconitine A were then verified in isolated prostatic smooth muscle strip tension tests. Prostatic smooth muscle strips ($0.2 \times 0.2 \times 1$ cm) isolated from healthy male New Zealand white rabbits were incubated in Krebs solution in the Multi Myograph System-610M with continuous 95% O_2 and 5% CO_2 at 37 °C. The bioactivity of the strips was verified by exposure to 60 mmol L^{-1} K^+-rich Krebs solution and Krebs solution as described in the previous section. Phenylephrine solution was then added to each chamber to stimulate the strips. When the tension was sustained, tamsulosin and bulleyaconitine A solution (1×10^{-8} to 1×10^{-4} mol L^{-1}) were added to each chamber and the concentration–response curves were generated.

Molecular docking study

The mechanisms underlying the effects of the screened compounds were simulated in molecular docking studies carried out using the Surflex-Dock Module of Sybyl-X 2.0. The X-ray crystal structure of α_{1A}-AR (PDB ID: 4iye) was retrieved from the Protein Data Bank with added hydrogen atoms and removed water molecules as well as the inhibitor. Powell's method was used to optimize the ligand files. The Gasteiger–Hückel charges and Tripos force field with 0.05 kcal (Å mol)$^{-1}$ convergence criterion were used to minimize energy. The ligands were docked into the rigid receptor protein using default parameters.

Results and discussion

Evaluation of α_{1A}/MNG stability

As bioactive compound grippers, α_{1A}/MNGs are thought to be highly efficient and stable. The cell membrane-cloaked nanoparticles reported in our previous study[28] were limited by poor stability after several cycles of use. Thus, consistent stability is a crucial property of biomaterials in real sample studies. To investigate their stability, three batches of α_{1A}/MNGs and α_{1A}/Fe_3O_4–OHs were prepared and added to standard tamsulosin

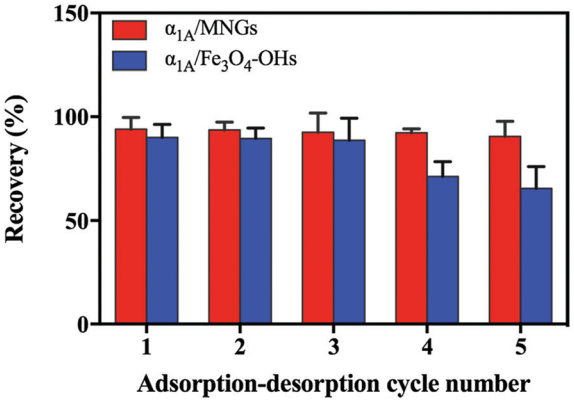

Fig. 2 Recoveries of α_{1A}/MNGs and α_{1A}/Fe_3O_4–OHs to tamsulosin.

solutions for use in all binding procedures described in the Experimental section. In this study, tamsulosin was selected as a positive control drug for α_{1A}-AR binding according to the literature.[50] As shown in Fig. 2, the recovery of α_{1A}/Fe_3O_4–OHs declined as the adsorption–desorption cycle increased. After five adsorption–desorption cycles, the recovery of α_{1A}/Fe_3O_4–OHs to tamsulosin was only 65.4%, which was a reduction of almost 25% compared to the recovery of α_{1A}/Fe_3O_4–OHs to tamsulosin in the first cycle. However, the adsorption capacity of α_{1A}/MNGs was reduced by only 3.4% after five adsorption–desorption cycles showing stable performance with no obvious decline in recovery. The recovery loss of α_{1A}/Fe_3O_4–OHs to tamsulosin is possibly due to the weak hydrophobic interaction between cell membrane and nanoparticles, which results in dissociation of the cell membrane during the washing and elution procedures. However, the free aldehyde groups on the surface of α_{1A}/MNGs nanoparticles react with the amino groups in phospholipids of the cell membrane *via* dynamic covalent bonding, which is much stronger than hydrophobic interactions and maintains the formation and stability of α_{1A}/MNGs. Thus, we concluded that α_{1A}/MNGs were stable for use in real applications.

Characterization of α_{1A}/MNGs

The physicochemical characteristics of α_{1A}/MNGs were investigated using DLS, FT-IR, XRD and VSM. DLS showed that the α_{1A}/MNGs were a slightly larger than the bare Fe_3O_4–CHO nanoparticles (550 nm *versus* 450 nm) (Fig. S1A†). Furthermore, the zeta potential of the α_{1A}/MNG surface was similar to that of the cell membrane-derived vesicles. We concluded that the surface of Fe_3O_4–CHO nanoparticles was effectively cloaked by the cell membrane and that the α_{1A}/MNGs were successfully prepared. The successful preparation of Fe_3O_4, Fe_3O_4–SiO_2 and Fe_3O_4–CHO was verified in FT-IR investigations. As shown in Fig. S1B,† the peak at 578 cm^{-1} was attributed to Fe–O stretching vibration. The characteristic absorption bands of the SiO_2 shell-layer were observed at 802, 948, and 1095 cm^{-1}, which were attributed to the stretching vibration of Si–O, Si–O–H and Si–O–Si, respectively. The peaks at 2830 cm^{-1} and 1720 cm^{-1} were attributed to the stretching vibration of C–H and C=O, respectively. Cell membrane cloaked nanoparticles' structures were confirmed by the appearance of C–H and C=O peaks at 2830 cm^{-1} and 1720 cm^{-1}, respectively and the appearance of C=N stretching at 1662 cm^{-1}. Hence, we concluded that α_{1A}/MNGs were successfully prepared.

The crystalline structures of Fe_3O_4, Fe_3O_4–CHO and α_{1A}/MNGs were investigated by XRD (Fig. S1C†). In the 20–80° 2θ range, six characteristic peaks of the three materials were observed. Their XRD patterns were consistent with that of the standard pattern of Fe_3O_4 evidenced by six diffraction peaks: (220), (311), (400), (422), (511), and (440) which were obtained in the JCPDS (Joint Committee on Powder Diffraction Standards)-International Center for Diffraction Data (JCPDS card: 19-629) file. Thus, we concluded that there were no changes in the physical absorption between Si–OH and the cell membrane in the Fe_3O_4 phase. Magnetic characteristics are vital for the application of prepared nanogrippers in screening and separating target compounds. The magnetic hysteresis loops of Fe_3O_4, Fe_3O_4–CHO and α_{1A}/MNGs are shown in Fig. S1D.† The magnetic hysteresis loops of the three materials exhibited Fe_3O_4, Fe_3O_4–CHO and α_{1A}/MNGs's magnetic properties with a saturation magnetization of 52, 28 and 15 emu g^{-1}, respectively. All three materials were highly susceptible to magnetic fields and were completely and rapidly (within a few seconds) separated from the complex sample by the application of an external magnetic field, even if there was a decrease in saturation magnetization between different kinds of materials resulting from the formation of SiO_2 and cell membrane shell-layers. As a result, the α_{1A}/MNGs quickly aggregated or formed a stable and homogeneous suspension following the application or removal of an external magnet during practical application.

The cell membrane-cloaking of Fe_3O_4–CHO nanoparticles was confirmed by TEM and confocal microscopy. As shown in Fig. 3A, TEM analysis of α_{1A}/MNGs revealed the typical core–shell structure of cell membrane-cloaked nanoparticles compared to bare Fe_3O_4–CHO cores. The cell membrane coating formed a ring around the bare Fe_3O_4–CHO core, indicating that the α_{1A}/MNGs were successfully prepared. Moreover, Fe_3O_4–CHO nanoparticles were constructed with a green fluorescent dye (FITC; excitation/emission 488 nm/520 nm) and cell membranes were labeled with a red fluorescent dye (DiI; excitation/emission 549 nm/565 nm). As shown in Fig. 3B and Fig. S2 (the bright-field images),† although there was quenching of the green fluorophore on the particles because of the magnetic core, the green and red fluorescence signals were clearly derived from Fe_3O_4–CHO cores and the cell membrane, respectively, and marked colocalization was observed. Overall, we concluded that the cell membranes were successfully translocated to the surface of Fe_3O_4–CHO nanoparticles.

Adsorption capacity of α_{1A}/MNGs

The significant binding properties of the α_{1A}/MNGs observed in the real application were investigated by static and selectivity studies. As shown in Fig. 4A, the adsorption capacity of

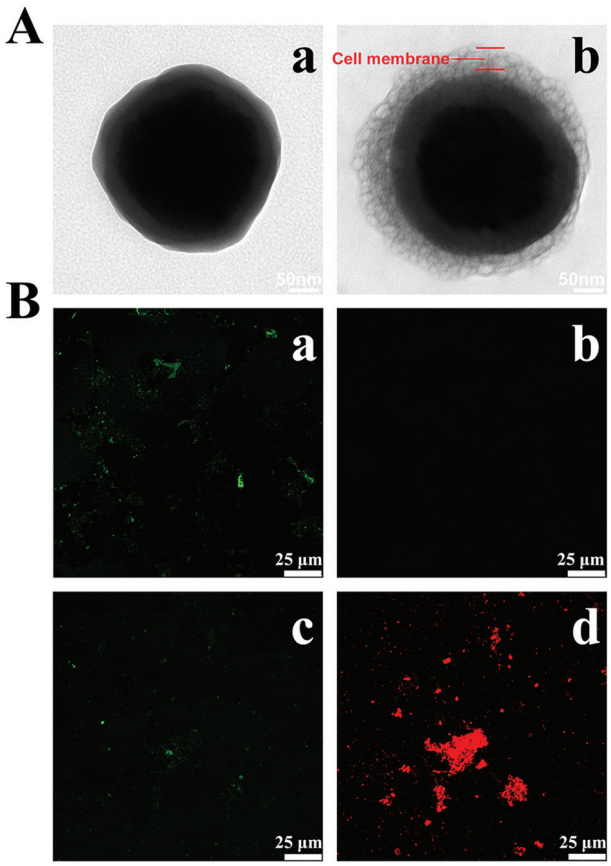

Fig. 3 TEM images of bare MNG cores (a) and α_{1A}/MNGs (b) (A); confocal microscopy images of MNG cores (a and b) and α_{1A}/MNGs (c and d) (green = nanoparticles cores, red = cell membrane) (B).

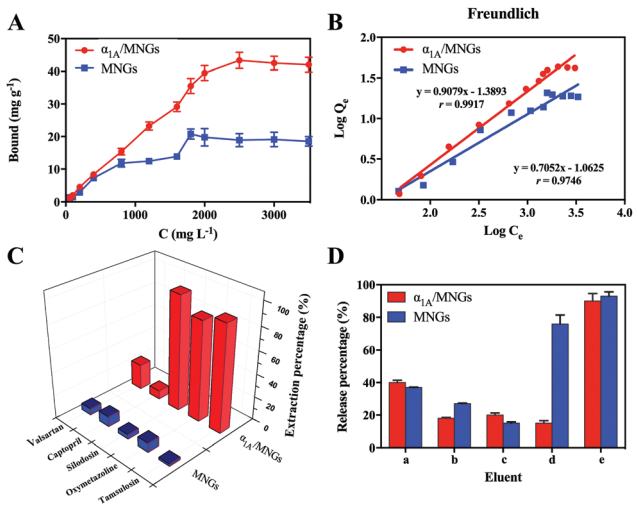

Fig. 4 Static adsorption isotherm results (A) and isotherm with Freundlich fit (B); extraction percentage of five compounds on both α_{1A}/MNGs and MNGs (C); release percentage of tamsulosin with five eluents on both α_{1A}/MNGs and MNGs: water (a), PBS (b), water–methanol (2 : 8, v/v, c), 0.1% acetic acid solution (d) and 1% acetic acid solution (e) (D).

tamsulosin by α_{1A}/MNGs increased rapidly at the start of the experiment and then slowed as the concentration of tamsulosin increased from 60 mg mL^{-1} to 2000 mg mL^{-1}. The adsorption capacity then became stable and reached a saturation plateau at 43.35 mg g^{-1}. Moreover, the α_{1A}/MNG adsorption was much higher than that of MNGs. The binding properties of α_{1A}/MNGs were further evaluated by processing of the binding data using Freundlich,[51] Langmuir,[52] Scatchard[48] and Dubinin–Radushkevich isotherms[53] (Fig. 4B and Table 1). The Freundlich isotherm (FI) model provided a perfect description of the static adsorption with the highest correlation coefficient (r, 0.9917 for α_{1A}/MNGs and 0.9746 for MNGs). FI is a widely used model based on eqn (2) and (3) as follows:

$$Q_e = K_F \times C_e^m \quad (2)$$

$$\lg Q_e = \lg K_F + m \lg C_e \quad (3)$$

where Q_e (mg g^{-1}) and C_e (mg L^{-1}) represent the amounts of free and bound tamsulosin, respectively. K_F, and m K_F represent adsorption capacity and m the heterogeneity index was constant. According to the FI equation, the K_F for α_{1A}/MNGs was 8.61 L mg^{-1} and m was 0.9079 (Table 1).

To investigate binding selectivity, α_{1A}/MNGs were pretreated with five different types of drugs: valsartan, captopril, silodosin, oxymetazoline and tamsulosin. Among them, silodosin,[54] oxymetazoline[55] and tamsulosin were chosen as the positive control drugs that act on the α_{1A}-AR and are bound by α_{1A}/MNGs, respectively. As shown in Fig. 4C, silodosin, oxymetazoline and tamsulosin were bound by α_{1A}/MNGs with high affinity and significantly higher recoveries than that achieved with MNGs. In contrast, valsartan and captopril were not bound by either α_{1A}/MNGs or MNGs. Overall, these results demonstrate that α_{1A}/MNGs exhibit strong selectivity and binding affinity for α_{1A}-AR-related drugs.

Optimization for α_{1A}/MNGs in the extraction procedure

The choice of eluent is important in the extraction procedure. To minimize adsorption of non-specific compounds by the membrane, the washing solvent and eluent were optimized. For optimal efficiency, five solvents (water, PBS, water–methanol (2 : 8, v/v), 0.1% acetic acid solution and 1% acetic acid solution) were utilized. As shown in Fig. 4D, 0.1% acetic acid solution exhibited a good washing efficiency with high desorption of the positive control drug from the MNGs. In addition, 1% acetic acid solution provided good desorption of tamsulosin from α_{1A}/MNGs. Therefore, 0.1% acetic acid solution and 1% acetic acid solution were selected as the washing solvent and eluent in the gripping procedure.

Method validation and real application of α_{1A}/MNGs to TCM samples

Under the optimized experimental conditions, we investigated a series of experimental parameters using this method. All analyses were performed three times using α_{1A}/MNGs from different batches. Satisfactory linearity was obtained for standard tamsulosin in the concentration range of 1–1000 mg L^{-1}

Table 1 Equations and parameters of adsorption isotherms of α_{1A}/MNGs and MNGs

Model	Equations and parameters	α_{1A}/MNGs	MNGs
Freundlich isotherm	$\lg Q_e = \lg K_F + m \lg C_e$		
	K_F (L mg^{-1})	8.61	8.94
	m	0.9079	0.7052
	r	0.9917	0.9746
Langmuir isotherm	$\frac{C_e}{Q_e} = \frac{1}{Q_{max}K_L} + \frac{1}{Q_{max}}C_e$		
	K_L	2.66×10^{-4}	9.46×10^{-4}
	Q_{max}	108.70	26.67
	r	0.8523	0.9586
Scatchard isotherm	$\frac{Q_e}{C_e} = \frac{Q_{max}}{K_d} - \frac{Q_e}{K_d}$		
	K_d (mg L^{-1})	5000	1429
	Q_{max} (mg g^{-1})	134.5	32.14
	r	0.6791	0.8132
Dubinin–Radushkevich isotherm	$\lg T_e = \lg T_{max} - K_{ad}\left(RT \lg\left(1 + \frac{1}{C_e}\right)\right)^2$		
	K_{ad} (mg^2 KJ^{-2})	2.9×10^{-3}	278.4
	Q_{max} (mg g^{-1})	22.76	—
	r	0.6882	0.5128

(r = 0.9997). The calculated limit of detection was estimated as three times the signal-to-noise ratio, which was equivalent to 0.4 mg mL^{-1}. The reproducibility of the biomaterials is a crucial property in actual sample application. Thus, six batches of α_{1A}/MNGs were prepared and added to standard tamsulosin solutions. The relative standard deviation (RSD) value for the recovery was less than 7.3%, showing better reproducibility and stability of α_{1A}/MNGs for gripping bioactive compounds from TCMs compared with that of our previous study.[28] These findings indicate the benefit of the covalent bonding method for the preparation of α_{1A}/MNGs.

The magnetic biomaterials generated in this study were designed to provide a rapid, simple, targeted and effective sample pretreatment technique for binding target compounds from complex mixtures. To determine the applicability of the proposed materials for this purpose, α_{1A}/MNGs were pretreated with RAA extract solution. As shown in Fig. 5, two main components of the RAA extract were bio-gripped by α_{1A}/MNGs, whereas a large number of components were discarded. The two bio-gripped components were identified as benzoylhypacoitine and bulleyaconitine A by TOFMS analysis. These results were verified by pretreatment of α_{1A}/MNGs with the corresponding commercially available reference solutions.

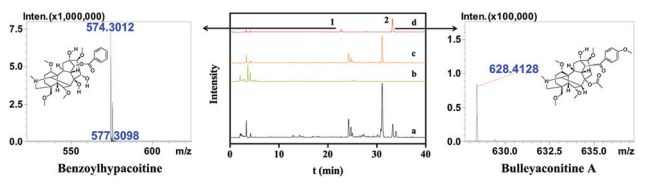

Fig. 5 Chromatograms of RAA extracts pretreated with α_{1A}/MNGs. Initial RAA extract solution (a), solution after loading (b), solution after washing (c), solution after eluting (d); TOFMS and chemical construction of peaks 1 and 2 in eluent.

Pharmacological effect

To verify the bioactivity of the bound compounds, isolated vascular ring tension assays were conducted using tamsulosin as a positive control (Fig. 6A). Compared to the positive control, benzoylhypacoitine and bulleyaconitine A both showed strong dose-dependent vasodilatation effects on the isolated Sprague Dawley rat antral circular smooth muscle strips which had been pre-contracted by exposure to phenylephrine. In addition, bulleyaconitine A exhibited extremely high bioactivity (100 ± 2.0%). Similar *in vitro* bioactivity investigations showed that bulleyaconitine A also evoked a concentration-dependent relaxation of prostatic smooth muscle strips pre-contracted by exposure to phenylephrine (Fig. 6B) compared with the effects of tamsulosin. Indeed, the maximum relaxation effect of bulleyaconitine A was 132 ± 2.0%, which was even higher than that of tamsulosin (119 ± 9.0%). Furthermore, bulleyaconitine A showed a gentle, slow and persistent relaxation effect compared to that of the positive control group. Hence, the high bioactivity of bulleyaconitine A and benzoylhypacoitine confirms the effective targeting and griping binding of α_{1A}/MNGs.

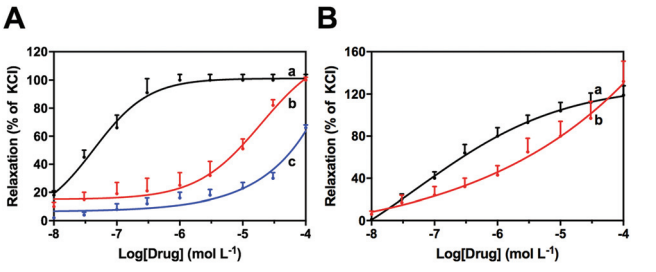

Fig. 6 Relaxant effects of tamsulosin (a), bulleyaconitine A (b) and benzoylhypacoitine (c) on isolated SD rat antral circular smooth muscle strips (A) and isolated male New Zealand white rabbit prostatic smooth muscle strips (B). All values are mean ± SEM, n = 6.

Molecular docking experiment

Molecular docking studies were conducted to investigate the interaction of benzoylhypacoitine and bulleyaconitine A with α_{1A}-AR, and to clarify the underlying mechanisms and binding models. Both compounds were docked into the active site of α_{1A}-AR (PDB ID: 4iye). Tamsulosin was utilized as a positive control drug to define the binding cavity. The maximum possible binding positions of benzoylhypacoitine and bulleyaconitin A were obtained. As shown in Fig. S3,† both benzoylhypacoitine and bulleyaconitin A bound to the same region of α_{1A}-AR and in a similar manner to that of tamsulosin. Thus, benzoylhypacoitine and bulleyaconitin A were validated as selective α_{1A}-AR blockers with high affinity.

Conclusion

In summary, we have developed a novel and highly stable functionalized nanoparticle-based cell membrane-cloaked strategy for targeting and gripping of bioactive compounds from TCM. Specifically, α_{1A}/MNGs were prepared using covalent bonding between cell membranes and Fe_3O_4–CHO nanoparticles. This technique represents significant progress in improving the quality and stability of these materials, with α_{1A}/MNG recovery found to be stable after five adsorption–desorption cycles. Moreover, we demonstrated the desirable morphological and physical characteristics, magnetic features, chemical composition and crystalline structure of the α_{1A}/MNGs. In addition, the binding capacity and specificity of α_{1A}/MNGs were successfully validated. FI isotherms accurately modeled the adsorption capacity of α_{1A}/MNGs. Ultimately, we showed that the bioactive compounds bulleyaconitine A and benzoylhypacoitine were effectively bound in the real application of α_{1A}/MNGs. The bioactivities of the screened compounds were validated in preliminarily pharmacological assays. Thus, our findings indicate that the unique function and enhanced stability of cell membrane-cloaked MNPs in binding bioactive compounds represent a promising platform for new drug discovery strategies. Furthermore, we show that aldehyde group modification further enhances the stability of the cell membrane-cloaked MNPs for the identification of natural products from complex matrixes. Therefore, the application of our findings will broaden the scope for integration of cell membranes with the nanoparticle platform.

Conflicts of interest

There are no conflicts to declare.

Acknowledgements

We gratefully acknowledge the National Natural Science Foundation of China (No. 81503033 and 81673398), the Natural Science Foundation of Shaanxi province (No. 2016JQ8016), the Fundamental Research Funds for the Central Universities (No. xjj2018222) and the World-Class Universities (Disciplines) and the Characteristic Development Guidance Funds for the Central Universities (No. PY3A012) for financial support.

Notes and references

1 M. A. Miller, S. Gadde, C. Pfirschke, C. Engblom, M. M. Sprachman, R. H. Kohler, K. S. Yang, A. M. Laughney, G. Wojtkiewicz, N. Kamaly, S. Bhonagiri, M. J. Pittet, O. C. Farokhzad and R. Weissleder, *Sci. Transl. Med.*, 2015, **7**, 183–314.
2 Y. Zhang, Q. Ni, C. Xu, B. Wan, Y. Geng, G. Zheng, Z. Yang, J. Tao, Y. Zhao, J. Wen, J. Zhang, S. Wang, Y. Tang, Y. Li, Q. Zhang, L. Liu, Z. Teng and G. Lu, *ACS Appl. Mater. Interfaces*, 2019, **11**, 3654–3665.
3 K. Cheng, Z. Sun, Y. Zhou, H. Zhong, X. Kong, P. Xia, Z. Guo and Q. Chen, *Biomater. Sci.*, 2013, **1**, 965–974.
4 M. Lewin, N. Carlesso, C.-H. Tung, X.-W. Tang, D. Cory, D. T. Scadden and R. Weissleder, *Nat. Biotechnol.*, 2000, **18**, 410.
5 B. Zheng, M. P. von See, E. Yu, B. Gunel, K. Lu, T. Vazin, D. V. Schaffer, P. W. Goodwill and S. M. Conolly, *Theranostics*, 2016, **6**, 291–301.
6 Y. Zhang, M. Nie, S. Shi, Q. You, J. Guo and L. Liu, *Food Chem.*, 2014, **146**, 56–64.
7 Z. M. Saiyed, S. D. Telang and C. N. Ramchand, *BioMagn. Res. Technol.*, 2003, **1**, 2.
8 K. K. Jain, *Drug Discovery Today*, 2005, **10**, 1435–1442.
9 Y. Tao, Y. Zhang, Y. Cheng and Y. Wang, *Biomed. Chromatogr.*, 2013, **27**, 148–155.
10 Y. Li, J. Xu, Y. Chen, Z. Mei and Y. Xiao, *J. Chromatogr. A*, 2015, **1425**, 8–16.
11 J. Xie, K. Chen, Ha.-Y. Lee, C. Xu, A. R. Hsup, S. Peng, X. Chen and S. Sun, *J. Am. Chem. Soc.*, 2008, **130**, 7542–7543.
12 S. Y. New, K. M. Aung, G. L. Lim, S. Hong, S. K. Tan, Y. Lu, E. Cheung and X. Su, *Anal. Chem.*, 2014, **86**, 2361–2370.
13 H. Groult, N. Poupard, F. Herranz, E. Conforto, N. Bridiau, F. Sannier, S. Bordenave, J. M. Piot, J. Ruiz-Cabello, I. Fruitier-Arnaudin and T. Maugard, *Biomacromolecules*, 2017, **18**, 3156–3167.
14 H. Gong, F. Chen, Z. Huang, Y. Gu, Q. Zhang, Y. Chen, Y. Zhang, J. Zhuang, Y.-K. Cho, R. H. Fang, W. Gao, S. Xu and L. Zhang, *ACS Nano*, 2019, **13**, 3714–3722.
15 Q. Zhang, D. Dehaini, Y. Zhang, J. Zhou, X. Chen, L. Zhang, R. H. Fang, W. Gao and L. Zhang, *Nat. Nanotechnol.*, 2018, **13**, 1182–1190.
16 C.-M. J. Hu, R. H. Fang, K.-C. Wang, B. T. Luk, S. Thamphiwatana, D. Dehaini, P. Nguyen, P. Angsantikul, C. H. Wen, A. V. Kroll, C. Carpenter, M. Ramesh, V. Qu, S. H. Patel, J. Zhu, W. Shi, F. M. Hofman, T. C. Chen, W. Gao, K. Zhang, S. Chien and L. Zhang, *Nature*, 2015, **526**, 118–121.

17 H.-W. Chen, Z.-S. Fang, Y.-T. Chen, Y.-I. Chen, B.-Y. Yao, J.-Y. Cheng, C.-Y. Chien, Y.-C. Chang and C.-M. J. Hu, *ACS Appl. Mater. Interfaces*, 2017, **9**, 39953–39961.
18 J. Li, X. Wang, D. Zheng, X. Lin, Z. Wei, D. Zhang, Z. Li, Y. Zhang, M. Wu and X. Liu, *Biomater. Sci.*, 2018, **6**, 1834–1845.
19 Q. Hu, Y. Bu, R. Cao, G. Zhang, X. Xie and S. Wang, *Anal. Chem.*, 2019, **91**, 13062–13070.
20 Z. Chai, X. Hu, X. Wei, C. Zhan, L. Lu, K. Jiang, B. Su, H. Ruan, D. Ran, R. H. Fang, L. Zhang and W. Lu, *J. Controlled Release*, 2017, **264**, 102–111.
21 X. Zhang, P. Angsantikul, M. Ying, J. Zhuang, Q. Zhang, X. Wei, Y. Jiang, Y. Zhang, D. Dehaini, M. Chen, Y. Chen, W. Gao, R. H. Fang and L. Zhang, *Angew. Chem., Int. Ed.*, 2017, **56**, 14075–14079.
22 Q. Jiang, Z. Luo, Y. Men, P. Yang, H. Peng, R. Guo, Y. Tian, Z. Pang and W. Yang, *Biomaterials*, 2017, **143**, 29–45.
23 J. Deng, S. Xu, W. Hu, X. Xun, L. Zheng and M. Su, *Biomaterials*, 2018, **154**, 24–33.
24 X. Wei, J. Gao, F. Wang, M. Ying, P. Angsantikul, A. V. Kroll, J. Zhou, W. Gao, W. Lu, R. H. Fang and L. Zhang, *Adv. Mater.*, 2017, **29**, 1701644.
25 T. D. T. Nguyen, A. Pitchaimani, M. B. Koirala, F. Muhammad and S. Aryal, *RSC Adv.*, 2016, **6**, 33003–33008.
26 F. Fontana, M. A. Shahbazi, D. Liu, H. Zhang, E. Mäkilä, J. Salonen, J. T. Hirvonen and H. A. Santos, *Adv. Mater.*, 2017, **29**, 1603239.
27 A. V. Kroll, R. H. Fang, Y. Jiang, J. Zhou, X. Wei, C. L. Yu, J. Gao, B. T. Luk, D. Dehaini, W. Gao and L. Zhang, *Adv. Mater.*, 2017, **29**, 1703969.
28 Y. Bu, Q. Hu, R. Ke, Y. Sui, X. Xie and S. Wang, *Chem. Commun.*, 2018, **54**, 13427–13430.
29 Q. Hu, Y. Bu, X. Zhen, K. Xu, R. Ke, X. Xie and S. Wang, *Chem. Eng. J.*, 2019, **364**, 269–279.
30 J. Sherwood, J. Sowell, N. Beyer, J. Irvin, C. Stephen, A. J. Antone, Y. Bao and L. M. Ciesla, *Nanoscale*, 2019, **11**, 6352–6359.
31 D. Jürgen, *Science*, 2000, **287**, 1960–1964.
32 S. G. Patching, *Biochim. Biophys. Acta, Biomembr.*, 2014, **1838**, 43–55.
33 S. Majd and M. Mayer, *Angew. Chem., Int. Ed.*, 2005, **44**, 6697–6700.
34 X. Ding, X. Chen, Y. Cao, D. Jia, D. Wang, Z. Zhu, J. Zhang, Z. Hong and Y. Chai, *J. Chromatogr. A*, 2014, **1359**, 330–335.
35 L. He, S. Wang and X. Geng, *Chromatographia*, 2001, **54**, 71–76.
36 Ł. Syga, D. Spakman, C. M. Punter and B. Poolman, *Sci. Rep.*, 2018, **8**, 13789.
37 N. S. K. Gunda, M. Singh, L. Norman, K. Kaur and S. K. Mitra, *Appl. Surf. Sci.*, 2014, **305**, 522–530.
38 C. Wang, G. Wang, Z. Wang and X. Zhang, *Chem. – Eur. J.*, 2011, **17**, 3322–3325.
39 J. Mann, *Nat. Rev. Cancer*, 2002, **2**, 143–148.
40 G. Kallifatidis, J. J. Hoy and B. L. Lokeshwar, *Semin. Cancer Biol.*, 2016, **40–41**, 160–169.
41 A. Bishayee and G. Sethi, *Semin. Cancer Biol.*, 2016, **40–41**, 1–3.
42 M. C. Wani, H. L. Taylor, M. E. Wall, P. Coggon and A. T. McPhail, *J. Am. Chem. Soc.*, 1971, **93**, 2325–2327.
43 S. M. Tolaney, W. T. Barry, C. T. Dang, D. A. Yardley, B. Moy, P. K. Marcom, K. S. Albain, H. S. Rugo, M. Ellis, I. Shapira, A. C. Wolff, L. A. Carey, B. A. Overmoyer, A. H. Partridge, H. Guo, C. A. Hudis, I. E. Krop, H. J. Burstein and E. P. Winer, *N. Engl. J. Med.*, 2015, **372**, 134–141.
44 M. E. Wall, M. C. Wani, C. E. Cook, K. H. Palmer, A. T. McPhail and G. A. Sim, *J. Am. Chem. Soc.*, 1966, **88**, 3888–3890.
45 K. M. Camacho, S. Kumar, S. Menegatti, D. R. Vogus, A. C. Anselmo and S. Mitragotri, *J. Controlled Release*, 2015, **210**, 198–207.
46 L. C. Pinheiro and J. M. Pisco, *Tech. Vasc. Interv. Radiol.*, 2012, **15**, 256–260.
47 B. Liu, D. Zhang, J. Wang, C. Chen, X. Yang and C. Li, *J. Phys. Chem. C*, 2013, **117**, 6363–6372.
48 Y. He, Y. Huang, Y. Jin, X. Liu, G. Liu and R. Zhao, *ACS Appl. Mater. Interfaces*, 2014, **6**, 9634–9642.
49 X. Xie, Q. Hu, R. Ke, X. Zhen, Y. Bu and S. Wang, *Chem. Eng. J.*, 2019, **371**, 130–137.
50 A. J. Noble, R. Chess-Williams, C. Couldwell, K. Furukawa, T. Uchyiuma, C. Korstanje and C. R. Chapple, *Br. J. Pharmacol.*, 1997, **120**, 231–238.
51 R. J. U. Andrew, M. Rampey II, G. T. Rushton, J. C. Iseman, R. N. Shah and K. D. Shimizu, *Anal. Chem.*, 2004, **76**, 1123–1133.
52 W. Xi, B. K. Shrestha and A. J. Haes, *Anal. Chem.*, 2017, **90**, 128–143.
53 R. Soltani, M. Dinari and G. Mohammadnezhad, *Ultrason. Sonochem.*, 2018, **40**, 533–542.
54 K. Kawabe, M. Yoshida, Y. Homma and Silodosin Clinical Study Group, *BJU Int.*, 2006, **98**, 1019–1024.
55 J. Akinaga, V. Lima, L. R. d. A. Kiguti, F. Hebeler-Barbosa, R. Alcántara-Hernández, J. A. García-Sáinz and A. S. Pupo, *Mol. Pharmacol.*, 2013, **83**, 870–881.